

ACCEPTED MANUSCRIPT • OPEN ACCESS

Association between NO₂ concentrations and spatial configuration: A study of the impacts of COVID-19 lockdowns in 54 US cities

To cite this article before publication: Man Sing Wong *et al* 2021 *Environ. Res. Lett.* in press <https://doi.org/10.1088/1748-9326/abf396>

Manuscript version: Accepted Manuscript

Accepted Manuscript is “the version of the article accepted for publication including all changes made as a result of the peer review process, and which may also include the addition to the article by IOP Publishing of a header, an article ID, a cover sheet and/or an ‘Accepted Manuscript’ watermark, but excluding any other editing, typesetting or other changes made by IOP Publishing and/or its licensors”

This Accepted Manuscript is © 2021 The Author(s). Published by IOP Publishing Ltd.

As the Version of Record of this article is going to be / has been published on a gold open access basis under a CC BY 3.0 licence, this Accepted Manuscript is available for reuse under a CC BY 3.0 licence immediately.

Everyone is permitted to use all or part of the original content in this article, provided that they adhere to all the terms of the licence <https://creativecommons.org/licenses/by/3.0>

Although reasonable endeavours have been taken to obtain all necessary permissions from third parties to include their copyrighted content within this article, their full citation and copyright line may not be present in this Accepted Manuscript version. Before using any content from this article, please refer to the Version of Record on IOPscience once published for full citation and copyright details, as permissions may be required. All third party content is fully copyright protected and is not published on a gold open access basis under a CC BY licence, unless that is specifically stated in the figure caption in the Version of Record.

View the [article online](#) for updates and enhancements.

Association between NO₂ concentrations and spatial configuration: A study of the impacts of COVID-19 lockdowns in 54 US cities

Man Sing Wong^{1,2}, Rui Zhu^{1,3*}, Coco Yin Tung Kwok¹, Mei-Po Kwan⁴, Paolo Santi^{5,6}, Chun Ho Liu⁷, Kai Qin⁸, Kwon Ho Lee⁹, Joon Heo¹⁰, Hon Li¹ and Carlo Ratti⁵

¹ Department of Land Surveying and Geo-Informatics, The Hong Kong Polytechnic University, Kowloon, Hong Kong

² Research Institute for Sustainable Urban Development, The Hong Kong Polytechnic University, Kowloon, Hong Kong

³ Senseable City Laboratory, Future Urban Mobility, Singapore-MIT Alliance for Research and Technology, 1 Create Way, 09-02 Create Tower, Singapore 138062

⁴ Institute of Space and Earth Information Science, The Chinese University of Hong Kong, Hong Kong, China

⁵ Senseable City Laboratory, Department of Urban Studies and Planning, Massachusetts Institute of Technology, Cambridge MA 02139 USA

⁶ Istituto di Informatica e Telematica del CNR, 56124 Pisa, Italy

⁷ Department of Mechanical Engineering, The University of Hong Kong, Hong Kong, China

⁸ School of Environment Science and Spatial Informatics, China University of Mining and Technology, China

⁹ Department of Atmospheric & Environmental Sciences, Gangneung-Wonju National University, Korea

¹⁰ Department of Civil and Environmental Engineering, Yonsei University, Korea

E-mail: felix.zhu@polyu.edu.hk

December 2020

Abstract. The massive lockdown of global cities during the COVID-19 pandemic is substantially improving the atmospheric environment, which for the first time, urban mobility is virtually reduced to zero, and it is then possible to establish a baseline for air quality. By comparing these values with pre-COVID-19 data, it is possible to infer the likely effect of urban mobility and spatial configuration on the air quality. In the present study, a time-series prediction model is enhanced to estimate the nationwide NO₂ concentrations before and during the lockdown measures in the United States, and 54 cities are included in the study. The prediction generates a notable NO₂ difference between the observations if the lockdown is not considered, and the changes in urban mobility can explain the difference. It is found that the changes in urban mobility associated with various road textures have a significant impact on NO₂ dispersion in different types of climates.

1
2
3
4
5 40 Submitted to: *Environ. Res. Lett.*
6
7
8 41 **1. Introduction**
9
10
11
12
13
14
15
16
17
18
19
20
21
22
23
24
25
26
27
28
29
30
31
32
33
34
35
36
37
38
39
40
41
42
43
44
45
46
47
48
49
50
51
52
53
54
55
56
57
58
59
60

In December 2019, the pandemic outbreak of severe acute respiratory syndrome coronavirus 2 (SARS-CoV-2) emerged in Wuhan, China, after which more than 10 million cases are confirmed and 500,000 deaths are resulted by 1 July 2020, and the pandemic also spread in over 250 countries in the world. Despite the progressive increase in the number of confirmed cases every day, the situation has become relatively stable in some countries after the massive lockdown is adopted and strict travel control measures are taken since March 2020 (Kucharski *et al.*, 2020). Due to the global lockdown, the *coronavirus disease 2019* (COVID-19) has undermined worldwide economies and triggered a global crisis due to great loss in the socioeconomic domain described by the United Nations (UNnews, 2020). It was predicted that global trade will decline by 13% to 32% and the annual global gross product is projected to decline by 24% (CRS, 2020). Additionally, a strict lockdown in China reduced global GDP by 3.5% and Chinese GDP by 21% (Guan *et al.*, 2020). Notwithstanding, the socioeconomic is chronically and devastatingly hit by the disease, and the environment has responded to the pandemic instantly (Fan *et al.*, 2020). The level of nitrogen dioxide (NO_2) is substantially reduced in the wake of COVID-19 (Mahato *et al.*, 2019). In Central China, NO_2 emission is decreased by 30% on a year-after-year basis during the Lunar New Year compared with the period from 2005-2019 (Earth Observatory, 2020). The reduction of air pollution including NO_2 is first identified appeared in Wuhan, and such phenomena are found in more and more cities and countries, and eventually it becomes a worldwide phenomenon (Venter *et al.*, 2020). Among 31 major cities in the world, a significant decline in NO_2 has been observed in almost two-thirds of the study area after the lockdown, including New York, Rome and Paris, implying that the transportation and anthropogenic activities in the cities mentioned above were massively lessened (Shrestha *et al.*, 2020). Epidemiological evidence suggested that the high incidence of respiratory disease and many death tolls should be attributed to the deteriorated air quality (Brauer *et al.*, 2010). For example, approximately 4.6 million individuals died from the disease annually due to the low air quality, as reported by the World Trade Organisation (Cohen *et al.*, 2017), and the lung tissue can be damaged by prolonged exposure to NO_2 , which is one of the contributors to the morbidity of asthma and lung cancer (Greenberg *et al.*, 2016; Khaniabadi *et al.*, 2017). Thus, it is of great significance to the enhancement of the atmospheric environment by grasping the evolutionary patterns of NO_2 and its causal factors appropriately (He *et al.*, 2020).

Road traffic can be regarded as the major contributor to NO_2 (Keuken *et al.*, 2009; Mohegh *et al.*, 2020; Palmgren *et al.*, 2007). The rise of NO_2 concentration might cause a certain type of diesel particulate produced by heavy vehicles such as buses, whereas nitrogen is produced by the gasoline-fueled passenger cars, particularly sensitive to long-range transport decomposition (Carslaw *et al.*, 2005; Heeb *et al.*, 2008). According to

an observation of the vehicle emission factors, it is found that the decreasing trend of NO₂ emission is the smallest and insignificant among other pollutants throughout the 12 years study period in Switzerland (Hueglin *et al.*, 2006), which suggests that the road traffic emission ratio in NO₂ increased during this period. A similar outcome means that NO₂ from the traffic emission is the key factor for generating ambient NO₂ concentration (Kurtenbach *et al.*, 2012). As such, NO₂ concentration will not be reduced substantially if only the NO_x exhaust system is improved without a significant reduction of traffic-related NO₂ emission. It is found that NO₂ had diurnal and seasonal variation as a function of traffic volumes alongside a major arterial (Kendrick *et al.*, 2015) and the traffic signals were related to the roadside air quality in Tokyo (Minoura *et al.*, 2010). Some studies also found that the change in NO₂ concentration is highly dependent on the traffic capacity and fuel decomposition, as well as the vehicle speed and fleet composition (Tang *et al.*, 2019). Nevertheless, it is reckoned that the improved air quality is mainly a result of the favourable meteorological conditions rather than the minimized anthropogenic activities because the pollutant diffusivity was an important factor closely related to meteorology (Wang *et al.*, 2020).

Another factor that contributes to NO₂ emission is traffic characteristics. By investigating the correlation between NO₂ and its emission factor, researchers speculated that the deviation of the contributing factors NO₂ emission resulted from the variability of the local road condition, the traffic pattern and the fleet composition (Chan *et al.*, 2004; Liu *et al.*, 2012). The road 300 km or above in length was featured by higher NO₂ concentration as shown by a study conducted in the Netherland (Velders *et al.*, 2009), and the study result is consistent with another finding that a higher NO₂ exposure was associated with the road length variability in Shanghai (Meng *et al.*, 2015). Moreover, the spatial distribution and the local variability of NO₂ concentration (Wang *et al.*, 2020) are analytically explored, and the results show that the local variation was mostly driven by regional differences between the ten most urbanized areas in the United States, which was consistent with the basic conditions of these urban regions, that is, comparatively denser traffic and frequent anthropogenic emission. Therefore, different spatio-temporal locations and the traffic characteristics have a significant influence on the level of NO₂, even though some of the emission features result from specific industrial activities. In the US metropolitan cities, the local NO₂ concentrations can be improved by reducing the road traffic even if there is a variability of estimation error in NO₂. Therefore, no effective prediction model has been developed for national NO₂ concentration yet (Lee *et al.*, 2019).

As a reliable and accurate method for mathematical modelling, Auto-Regressive Integrated Moving Average (ARIMA) has been widely applied to short-term time-series trend analysis and its frequent application in the prediction from multiple perspectives. For instance, it was adopted in the study trying to make an accurate forecast of wind speed at wind power plants and ensure the overall stability and security of the power system (Singh *et al.*, 2019). Likewise, the time-series trend is explored to predict the capacity of electricity generation (Haiges *et al.*, 2017). In other disciplines, the statistical

1
2
3
4
5
6
7
8
9
10
11
12
13
14
15
16
17
18
19
20
21
22
23
24
25
26
27
28
29
30
31
32
33
34
35
36
37
38
39
40
41
42
43
44
45
46
47
48
49
50
51
52
53
54
55
56
57
58
59
60
4
tool was adopted to detect financial crisis events that act as the precursor of the market regime (Faranda *et al.*, 2015). Apart from the modelling platform of Geographic Information Systems (GIS) for spatial clustering and statistical analysis, the spatial distribution and the association between infectious diseases and NO₂, and between the traffic flow and the number of people moving trajectory are also identified (Yongjian *et al.*, 2020). The assessment of the traffic related-GIS parameters such as the lengths of the major road segment and the traffic intensity can help reveal the long-term trend of NO₂ and their emission ratio related to the road traffic activities, and the impact on NO₂ can be visualized using the GIS platform (Shon *et al.*, 2011). With the use of predictive data based on ARIMA, the spatial transmissions of the pandemic disease can be forecasted regarding the spatial allocation of medical resources and the implementation of mitigating control measures (Lakhani, 2020; Singer *et al.*, 2020).

This paper is organized as follows. Section 2 enhances a time-series prediction model to predict NO₂ concentrations accurately and proposes four indices to present the characteristics of road networks. Section 3 introduces data collection, presents the changes of NO₂ concentration after lockdown, and explores the impacts of road networks and regional climates on NO₂ concentration. Finally, Section 4 makes a discussion and conclusion.

2. Methods

2.1. NO₂ difference between observation and prediction

The NO₂ concentration records before lockdown will be used to train historical patterns that contain seasonal and cyclic time-series information, and the SARIMAX model will be used to predict the NO₂ concentration. In this case, a prediction following historical patterns will not integrate with the new evolution after lockdown measures. Under the circumstance, two definitions are proposed to investigate the evolution:

- NO₂ difference denoted by Δd calculates the difference between the observed and predicted NO₂ concentration at a station after lockdown; and
- NO₂ change denoted by Δc calculates the difference of the mean NO₂ concentration before lockdown and that after lockdown based on observation or prediction.

Particularly, Δd can be significant as a result of the changes of urban mobility during the implementation of lockdown measures. Thus, we can investigate the relationship between Δd and the changes of urban mobility (Δm) subject to a baseline before lockdown.

2.2. Seasonal Autoregressive Integrated Moving Average with eXogenous factors (SARIMAX)

The general Auto-Regressive Integrated Moving Average (ARIMA) model consists of three parts, namely autoregression (AR), differencing (I) and moving average (MA),

1
2
3
4
5
6
7
8
9
10
11
12
13
14
15
16
17
18
19
20
21
22
23
24
25
26
27
28
29
30
31
32
33
34
35
36
37
38
39
40
41
42
43
44
45
46
47
48
49
50
51
52
53
54
55
56
57
58
59
60

5

¹⁵⁹ and the model can be presented as follows:

$$\text{ARIMA}(p, d, q) \quad (1)$$

¹⁶¹ where p denotes the order of auto-regressive model, d represents the order of difference,
¹⁶² and q is the order of moving average model. Nonetheless, seasonal patterns cannot be
¹⁶³ established by introducing an ordinary ARIMA model. To address this problem, the
¹⁶⁴ Seasonal Auto-Regressive Integrated Moving Average (SARIMA) includes the seasonal
¹⁶⁵ parameters for the auto-regressive, differencing and moving average terms, and the time
¹⁶⁶ step for modelling the periodic time-series pattern:

$$\text{ARIMA}(p, d, q)(P, D, Q)_t \quad (2)$$

¹⁶⁸ where P denotes the order of seasonal auto-regressive model, D denotes the order of
¹⁶⁹ seasonal differencing, Q is the order of seasonal moving average model, and t refers to the
¹⁷⁰ time step parameter for seasonality. Furthermore, Seasonal Autoregressive Integrated
¹⁷¹ Moving Average with eXogenous factors (SARIMAX) can be used to analyze the time-
¹⁷² series data with additional variables in the regression operation ([Valipour, 2015](#)).

$$\text{ARIMAX}(p, d, q)(P, D, Q)_t \quad (3)$$

¹⁷⁴ In this study, the time-series NO₂ measurements of 56 stations in the US were modelled
¹⁷⁵ using the SARIMAX model based on the exogenous weather variables including air
¹⁷⁶ temperature, air pressure, relative humidity, wind speed and percentage of cloud
¹⁷⁷ coverage. Since there might be more than one seasonal pattern for the time-series NO₂
¹⁷⁸ data, six Fourier series with different periods were also included as exogenous variables
¹⁷⁹ (number of days = {15, 30, 90, 180, 365}), and 7 days (one week) was deemed to be the
¹⁸⁰ seasonal time step t in the SARIMAX model.

¹⁸¹ Before the SARIMAX modelling is performed, the randomness and normality
¹⁸² were tested with Ljung–Box test and Jarque-Bera test. The Augmented Dickey-
¹⁸³ Fuller (ADF) test and the Osborn, Chui, Smith, and Birchenhall (OCSB) tests were
¹⁸⁴ performed to determine the seasonally varying parameters (d and D) of the time series
¹⁸⁵ respectively. Canova-Hansen test was conducted to determine the time step parameter
¹⁸⁶ (t) for seasonality. Then, a stepwise approach ([Hyndman et al., 2008](#)) was adopted
¹⁸⁷ for optimizing the other parameters (i.e., p , q , P , and Q) of the SARIMA model by
¹⁸⁸ minimizing the Akaike information criterion (AIC) value. The optimized parameters
¹⁸⁹ were introduced for the NO₂ prediction in this study. Python 3.7 and the *statsmodels*
¹⁹⁰ package ([State Space Methods, 2020](#)) were used for training and prediction.

¹⁹¹ 2.3. Impacts of road networks on vehicle emission

¹⁹² As traffic is one of the major sources of NO₂, in the present study, four indices are
¹⁹³ adopted to explain the characteristics of road networks in a 3km-radius circular area
¹⁹⁴ centered at each air quality monitoring station (Figure 1a), which are used for correlation
¹⁹⁵ analysis between NO₂ difference after lockdown. The four indices are enumerated as
¹⁹⁶ follows: (i) n_{nd} denotes the number of road intersections, (ii) c_{nd} presents the number of

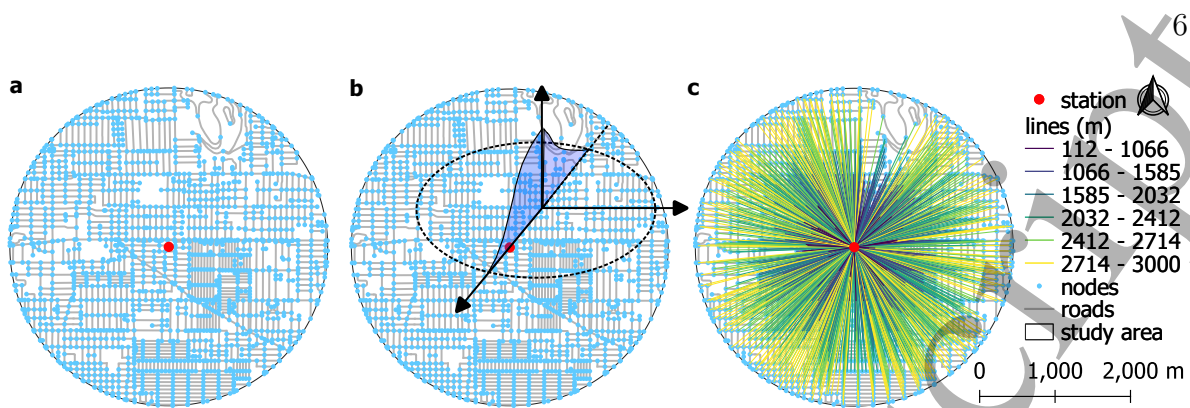


Figure 1. Methods to estimate the impact of road networks on NO_2 at stations. (a) The nodes and edges of a road graph g centered at an air quality station with a 3km radius. (b) The dispersion of NO_2 from an intersection to the station following a Gaussian distribution function. (c) The distances between the intersections of road networks and the station.

the road segments at all the intersections, (iii) s_{rd} stands for the total length of the road networks, and (iv) n_{rd} is the number of the road segments. It is crucial for proposing n_{nd} since vehicles often stop at the intersections because of the traffic lights, which leads to the accumulation of a considerable amount of the emissions during idling (Minoura *et al.*, 2010). In comparison, c_{nd} shall be more representative than n_{nd} because the number of roads connecting at each intersection is counted that may indicate temporary stopping more confidently. For example, vehicles are more likely to be parked at an intersection of two roads than a single road with the same traffic volume. s_{rd} also plays a big part since it affects traffic flows fundamentally. The four indices are thus organized as $i = \{n_{nd}, c_{nd}, s_{rd}, n_{rd}\}$. In the study, G denote a topological graph of roads that edges $E = \{e\}$ connect with each other by associating with the nodes $O = \{o\}$, getting $G = \{E, O\}$. Notably, n_{nd} is different from the number of nodes denotes by $num(O)$ because only two edges connecting through a node means they are the same road essentially, which is caused by the data format. Thus, n_{nd} and c_{nd} are counted when a node at least associates with at least edges.

However, based on the four indices, it is estimated that the dispersion of vehicle emissions at road networks has homogeneous impacts on stations' air quality when the spatial distance between them is taken into consideration. To make a better estimation, in the present study, it is assumed that the dispersion of each index follows a Gaussian distribution from each element of the index to the station (Figure 1b, Equation 4).

$$y = y_0 + Ae^{-\frac{(x-xc)^2}{2w^2}} \quad (4)$$

In the function, y_0 denotes the offset and xc is the center, both equalling 0 to present a normalized Gaussian. A is the *amplitude* to denote the magnitude of the element, w implies the *width* to control the speed of the dispersion, and x stands for the distance from the element to the station (Figure 1c). When computing n_{rd} and s_{rd} enriched with the Gaussian function, x is the distance from the middle point of the road segment to the station, as an approximation. Then, the total impacts of all the elements of an

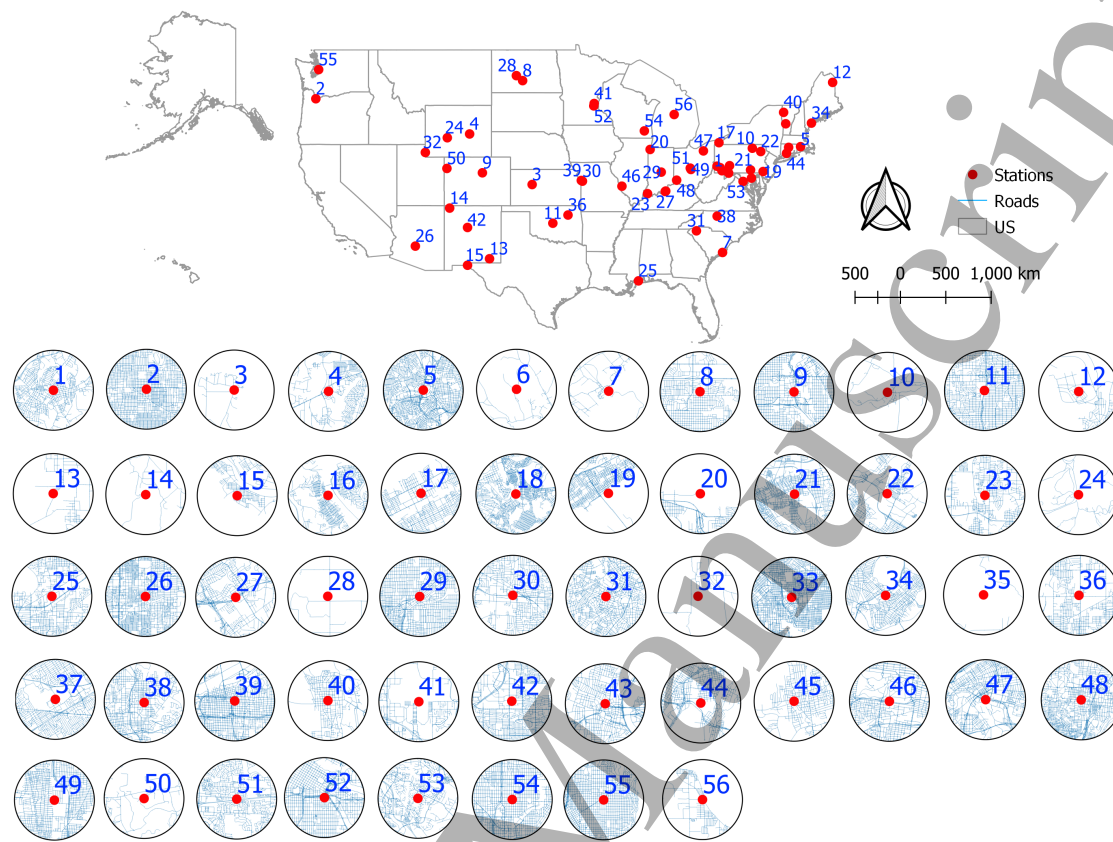


Figure 2. Locations of 56 air quality stations across the United States. Each circular area has a 3km radius centered at the stations, which are presented as the red dots with IDs. The densities of the road networks are diverse across the whole area.

No.	Climate	Station ID
1	Costal	5, 7, 19, 20, 25, 33, 34, 44, 53–55
2	Inland	1–4, 6, 8–18, 21–24, 26–32, 35–52, 56
3	Arid	3, 4, 8, 9, 11, 13–15, 24, 26, 28, 32, 42, 50
4	Humid	1–2, 5–7, 10, 12, 16–23, 25, 27, 29–31, 33–41, 43–49, 51–56
5	Hot	1–3, 5–7, 10, 11, 13–23, 25–27, 29–31, 33, 35–39, 42–44, 46–49, 51, 53, 55
6	Cold	4, 8, 9, 12, 24, 28, 32, 34, 40, 41, 45, 50, 52, 54, 56

Table 1. The station IDs are listed in six different climate types.

index at a station can be accumulated (Equation 5).

$$Y = \sum y = \sum_{m=1}^n g(A_m, x_m, w) \quad (5)$$

A set of abbreviations and their definitions are summarized in Table 2 for clear presentation of this study.

No.	Abbre.	Definition
1	Δd	NO ₂ difference: the predicted NO ₂ concentration minus the observed NO ₂ concentration at a station after lockdown
2	e	relative error: Δd divided by the observed NO ₂ concentration
3	Δc	NO ₂ change: the mean NO ₂ concentration after lockdown minus that before lockdown
4	Δc_p	NO ₂ change in percentage: Δc divided by the mean NO ₂ concentration before lockdown
5	Δm	the mean change of urban mobility subject to a specific day before lockdown; $\{\Delta m_w, \Delta m_r, \Delta m_t\}$ are the changes of mobility for <i>workplace</i> , <i>recreation</i> , and <i>public transit</i>
6	n_{nd}	the number of road intersections
7	c_{nd}	the number of the road segments connecting at all the intersections
8	s_{rd}	the total length of the road networks
9	n_{rd}	the number of the road segments
10	Δm_{rd}	$\Delta m_{rd} = s_{rd} \cdot \Delta m_w$

Table 2. Definitions of the abbreviations used in this study.

2.4. Data

Daily NO₂ observations at 56 stations in 54 cities across the US are derived from the *Air Quality Open Data Platform* during a period from June 2014 to May 2020 ([AQODP, 2020](#)), which are complemented by the geographical coordinates. The weather data taken as exogenous factors in the SARIMAX model are collected from OpenWeatherMap ([Open Weather, 2020](#)) with the coordinates of the 56 NO₂ stations. The *COVID-19 Community Mobility Reports* from Google provides *daily* mobility changes in percentage subject to the baseline on 15 February 2020 ([Google, 2020](#)), indicating user mobility in Google Maps during the COVID-19 pandemic. Mobility is aggregated and anonymized as six categorical purposes, including retail and recreation, groceries and pharmacies, parks, transit stations, workplaces, and residences. The originally collected NO₂ data and the mobility data have the same temporal resolution on one day, so that preprocessing is not needed. The study is based on the data collection between 15 February 2020 and 6 May 2020, which is the last day of the NO₂ data. Road networks in the US are acquired from OpenStreetMap ([OpenStreetMap, 2020](#)).

3. Results

3.1. NO₂ change after lockdown

Figure 2 presents 56 NO₂ stations in the US, covering a large geographical space, and Table 1 summarizes six climate types that prevail at the stations according to [National Weather Service \(2020\)](#). The stations are located in various micro-environments with

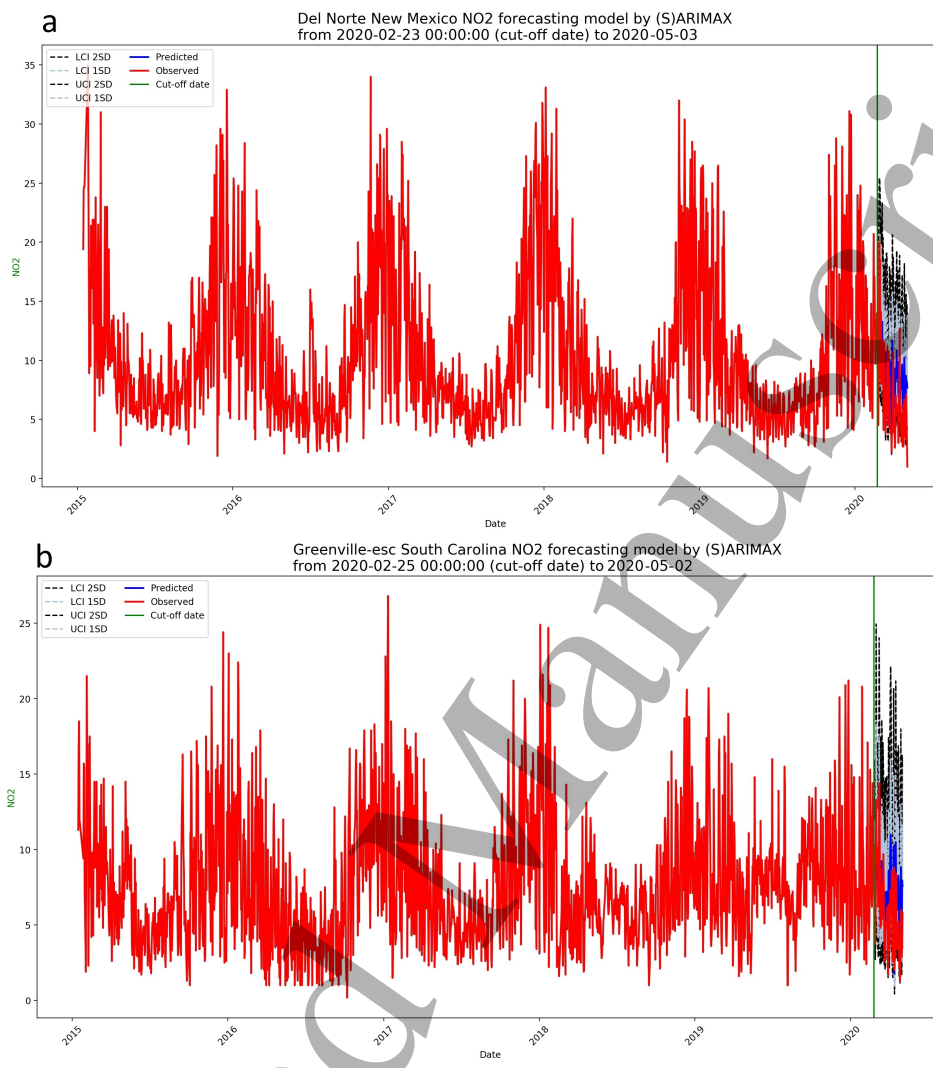


Figure 3. Prediction of the two selected sites. (a) Site located at Del Norte, New Mexico. (b) Site located at Greenville, South Carolina.

different road networks, and they are located in urban or rural areas of those cities that implement lockdown when the COVID-19 pandemic becomes quite severe. The training has been done at each station since June 2014. Then, the SARIMAX model is used to predict *daily* NO₂ at each station from the start of lockdown to the end of lockdown.

Two predictions are made, with one prediction period starting 60 days ($n=60$) before the lockdown and ending a number of days after the lockdown (until 6 May 2020), and the other prediction period is starting 30 days ($n=30$) before the lockdown and ending a number of days after the lockdown. Figure 3 visualizes prediction results of two selected sites that the red curves (observation) present a seasonal and periodical pattern, which are lower than the blue curves (prediction). The difference between the blue and red curves (i.e., NO₂ difference) confirms our hypothesis that the prediction has not incorporated the disruption of lockdown and can be explained by the reduction of mobility.

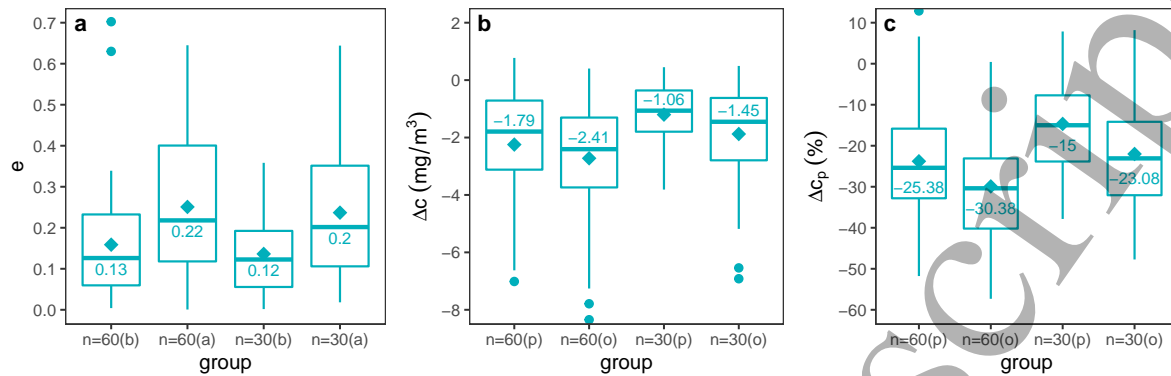


Figure 4. Relative errors of NO_2 prediction and statistics of NO_2 change. The numbers in each plot are the medians of statistics at the 50th percentile. The training has been implemented since 2014 at each station and the two predictions start from 60 days ($n=60$) and 30 days ($n=30$) before the lockdown dates. (a) Relative errors of the predicted NO_2 concentrations (e) at the 56 stations respectively before (b) and after (a) lockdown. (b) NO_2 changes (Δc) obtained from prediction (p) and observation (o). (c) NO_2 changes in percentage (Δc_p) obtained from prediction (p) and observation (o).

Figure 4a provides the distribution of the *mean* relative errors (e) of the prediction at all the stations. Evidently, the errors before lockdown (b) are smaller than after lockdown (a), with the medians at $e=0.13$ for $n=60$ and $e=0.12$ for $n=30$, respectively. It suggests that satisfactory prediction accuracy is achieved prior to the lockdown accordingly. When the lockdown was activated, the medians become larger at $e=0.22$ for $n=60$ and $e=0.20$ for $n=30$, which indicates that it is challenging to obtain accurate prediction caused by disruptive lockdown measures. Besides, both errors for $n=30$ are slightly smaller than that for $n=60$, probably because $n=60$ has a longer prediction time while $n=30$ allows an additional 30-day training that better incorporates the most recently seasonal variation into the prediction.

To probe into the impact of the lockdown measures, in the present study, the NO_2 changes before and after lockdown for the 56 stations based on prediction (p) and observation (o) are calculated, respectively. It is found that many stations have undergone a substantial reduction after lockdown in view of the changes of absolute values (Δc) (Figure 4b), which become more significant when conversion into percentages that Δc_p equals Δc divided by the mean concentration before lockdown (Figure 4c). Specifically, the observation suggests that half of the NO_2 measurements decreased at least with $-1.45 \text{ mg}/\text{m}^3$ for $n=30$ and $-2.41 \text{ mg}/\text{m}^3$ for $n=60$ (Figure 4b), which is equivalent to a 23.08% and 30.38% reduction of the NO_2 concentration before lockdown. Meanwhile, the predicted number is slightly larger than the observation.

According to the *COVID-19 Community Mobility Reports* from Google that provides relative urban mobility subject to a baseline before lockdown in each city, all the involved cities have shown a huge decrease in the mobility for *workplace* with $|\Delta m_w| > 20\%$, in which Seattle, Ashburn, Burlington, and Minneapolis have witnessed the largest reduction with $|\Delta m_w|$ equalling 41%, 38%, 36%, and 33%, respectively

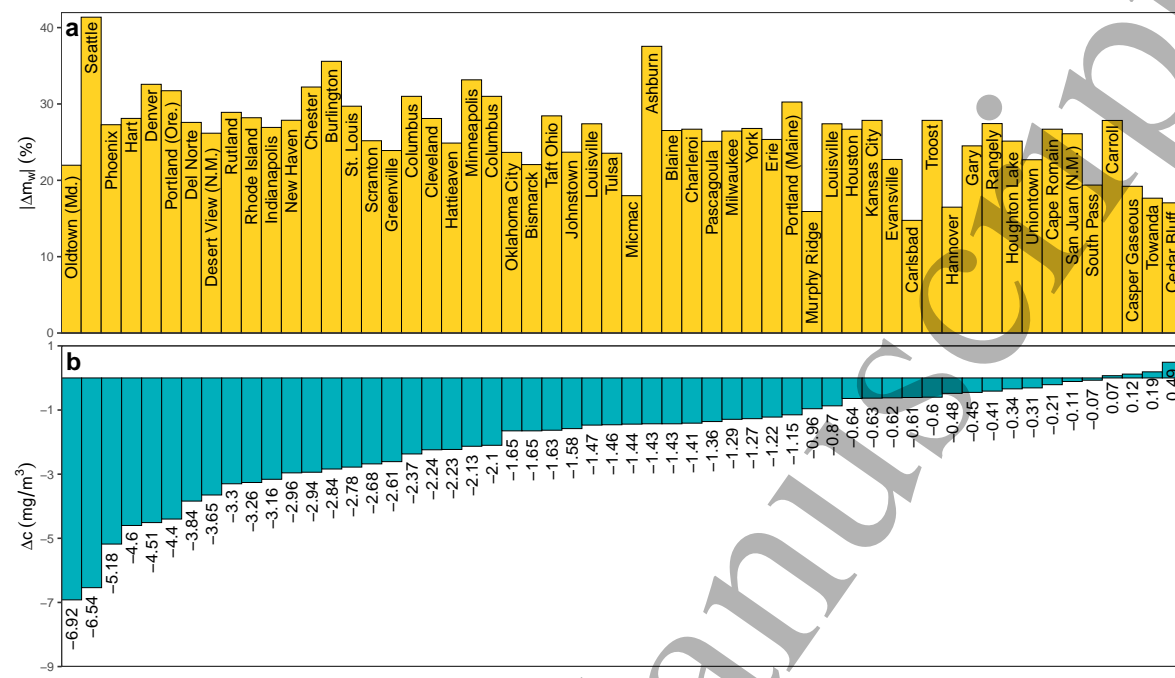


Figure 5. Changes of urban mobility and NO₂ difference in each individual city. (a) Absolute decrease of urban mobility for workplace ($|\Delta m_w|$). (b) NO₂ change (Δc) after lockdown, corresponding to the city in the x-axis of (a).

(Figure 5a). By inspecting each station, the observation suggests that a considerable reduction of NO₂ after lockdown is realized in most cities, while a tiny increase is found in four cities quite unexpectedly (Figure 5b). Notably, the changing trend of $|\Delta m_w|$ is unclear with the decrease of Δc , which stimulates our motivation to explore the influential factors.

3.2. Association between urban mobility and NO₂ difference

Considering the vehicle emission is one of the largest resources of NO₂, a significant reduction of urban mobility during the pandemic is supposed to have impacts on the changes of NO₂ in cities, which focuses on a detailed investigation by contrast with other studies at regional and national scales. Based on the *COVID-19 Community Mobility Reports*, the Pearson correlation analysis between the NO₂ difference (Δd) and the averaged mobility changes (Δm) is made, in categories of $n=30$ (Figure 6a) and $n=60$ (Figure 6b). It shows that the mobility for *workplace* decreases significantly in all cities ($-40\% \leq \Delta m_w \leq -15\%$), which validates a moderate and negative correlation with Δd in both groups (the Pearson correlation coefficient $R=-0.47$, $p < 0.05$). Similarly, the mobility for *recreation* has shown a considerable decrease in a vast majority cities ($-30\% \leq \Delta m_c \leq 1\%$), having a weak and negative correlation with Δd ($R=-0.37$ for $n=30$ and $R=-0.40$ for $n=60$). In comparison, the greatest decrease in *transit* mobility is observed in almost all the cities ($-50\% \leq \Delta m_t \leq 5\%$), which contributes to a weak and negative correlation ($R=-0.32$ for $n=30$ and $R=-0.34$ for $n=60$) (Figure 6).

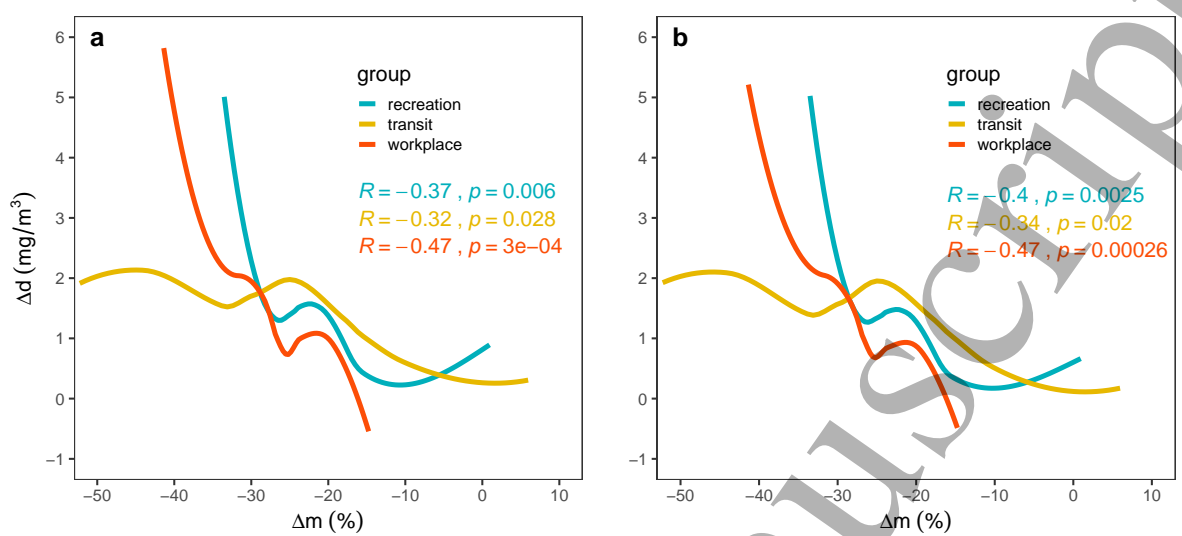


Figure 6. The Pearson correlation coefficients (R) and the significance (p) between the changes of the three mobilities (Δm) and NO_2 difference (Δd) after lockdown. (a) Correlations obtained from $n=30$. (b) Correlations obtained from $n=60$.

As an expectation, a small increase of $\Delta m_c = 0.94\%$ and $\Delta m_c = 5.95\%$ is revealed in the *recreation* mobility for the Cedar Bluff State Park in Kansas and the *transit* mobility for Murphy Ridge in Wyoming, respectively. It is reasonable since some populations may deliberately choose not to travel to crowded locations and move to rural areas as temporary residences such as parks. Three implications can also be induced by the results. Firstly, the lockdown policy helps reduce urban mobility for *recreation*, *transit*, and *workplace* greatly during the pandemic, leading to a considerable reduction of NO_2 . Secondly, the correlations between Δm and Δd , even though not robustly significant, suggest the validation of the hypothesis that the difference of NO_2 has resulted from the changes in urban mobility. Last but not least, other factors such as road characteristics or local climates may also affect the changes of NO_2 since the current correlations are not significantly strong.

3.3. Impacts of road networks on NO_2 concentration

As the urban mobility restraint by road networks, in the present studies, it is proposed that the road characteristics, such as the density of road networks, may have notable impacts on emission. Therefore, three static indices are put forth to represent road characteristics $i = \{n_{nd}, c_{nd}, s_{rd}\}$: (i) the number of road intersections n_{nd} , (ii) the total number of the road segments connecting at all the intersections c_{nd} , and (iii) the total length of the road networks s_{rd} . Figure 7 demonstrates the correlations between i and Δd , categorizing into two groups of $n=30$ and $n=60$. It is pointed out that both groups obtain somewhat strong and positive correlations that the coefficients $R = \{0.54, 0.54, 0.60\}$ for $n=30$, resulting a better performance than $(\Delta m, \Delta d)$ in Figure 6. It can be explained that a larger indicator in i makes a more significant effect

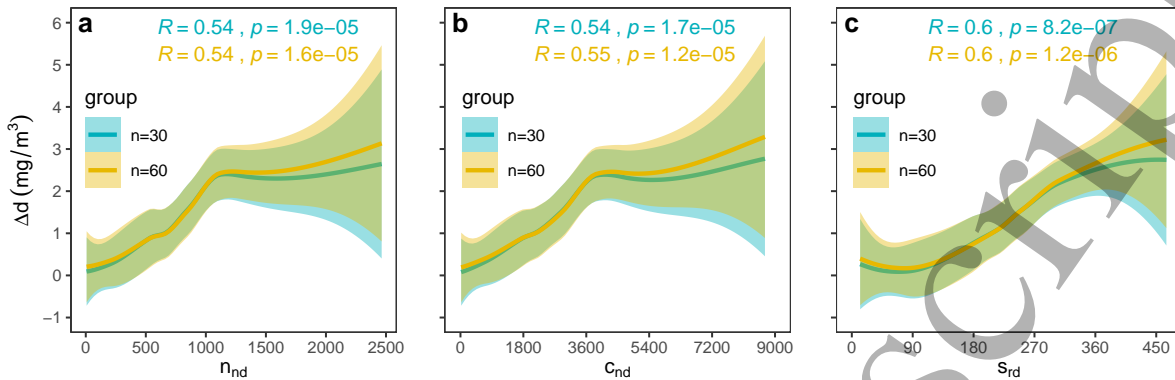


Figure 7. Pearson correlation coefficient (R) between Δd and three indices to represent innate characteristics of road networks. The buffer areas represent the confidence intervals. (a) The number of the road intersections n_{nd} . (b) The total number of road segments connecting at all the intersections c_{nd} . (c) The total length of road networks s_{rd} .

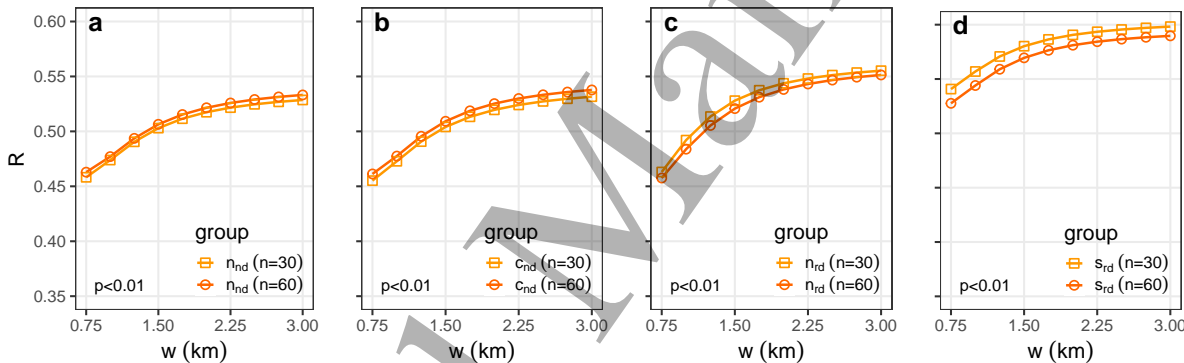


Figure 8. Pearson correlation coefficient (R) between the four indices of road networks (c_{nd} , n_{nd} , s_{rd} , n_{rd}) and Δd . w in the x-axis represents the width of the Gaussian function used to estimate the impact of the four indices on weather stations, and R in the y-axis has $p \leq 0.01$. (a, b, c, d) Correlations are based on $n=30$ and $n=60$.

on the changes of NO_2 after lockdown, suggesting that road networks' characteristics can greatly affect Δd . However, the three indicators treat intersections and roads with homogeneous impacts on the air quality stations, regardless of the spatial distance between the roads and stations.

To make the indices more representative, we used a Gaussian function $y = \sum g(A, x, w)$ to estimate the dispersion of NO_2 from the vehicle emission, in which A represents the magnitude of the road property, x denotes the distance from roads to the NO_2 station, and w indicates the width of the function. In addition, another road index named n_{rd} is initiated, which means that the dispersion associated with the road follows the Gaussian distribution but ignoring the characteristics of the road length to compare with the performance of s_{rd} . Figure 8 shows the coefficient curves between $i = \{n_{nd}, c_{nd}, s_{rd}, n_{rd}\}$ and Δd , comparing between $n=30$ and $n=60$. Overall, all the curves grow steadily and approach the upper bounds gradually with an increase of w . Particularly, c_{nd} and n_{nd} share the same growing trend with the increase of w

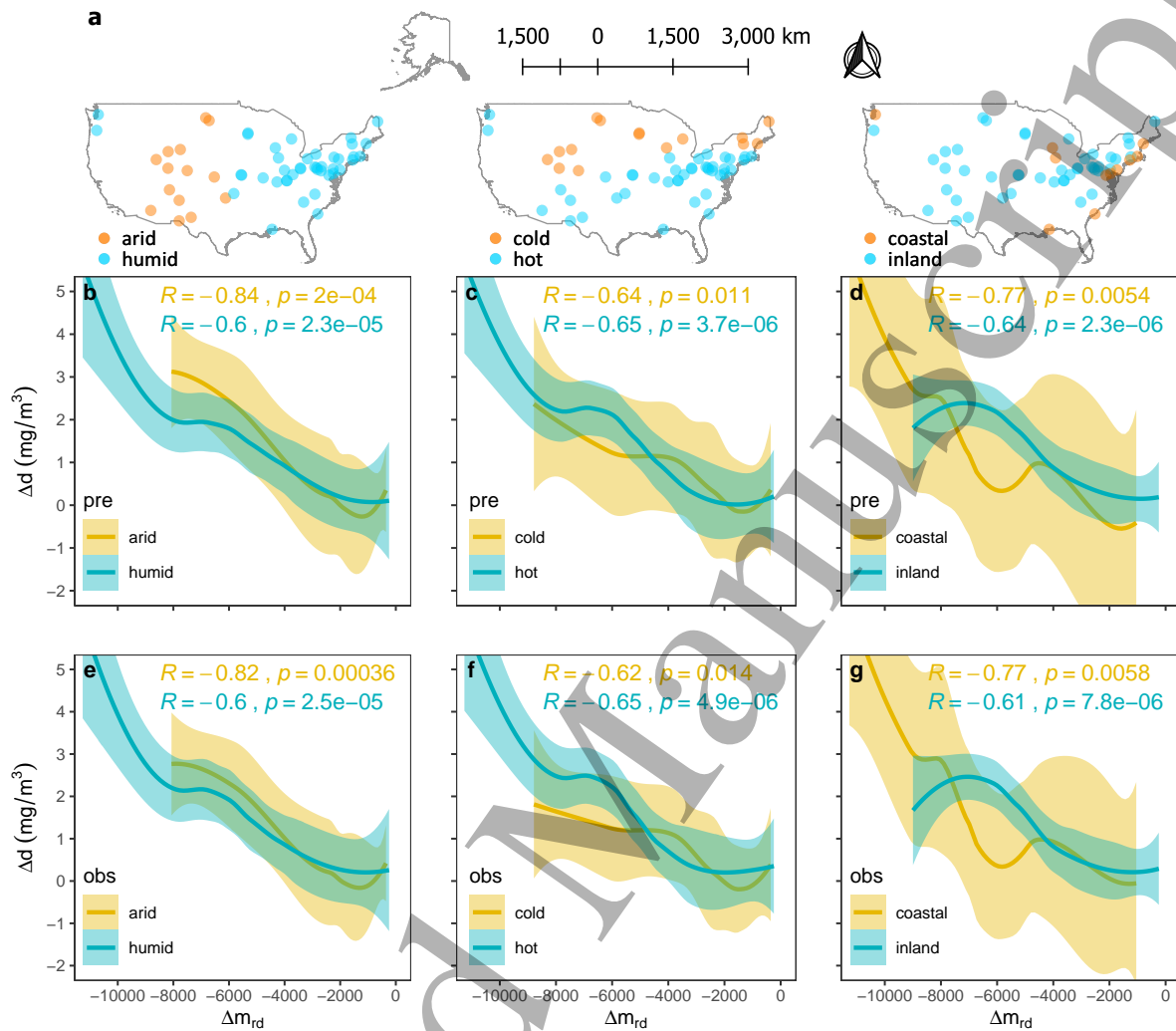


Figure 9. Pearson correlation coefficient (R) between Δd and Δm_{rd} estimated by the Gaussian function ($w = 3\text{km}$). The buffer areas symbolize the confidence intervals. (a) Stations are located at a place with six types of the climate. (b, c, d) R is derived from $n=30$. (e, f, g) R obtained on the condition of $n=60$. (b, e) Stations are in the arid and humid climates. (c, f) Stations are in the hot and cold climates. (d, g) Stations are in the coastal and inland climates.

that their $R_{max} < 0.55$ (Figure 8a, Figure 8b). Also, c_{nd} is insignificantly larger than n_{nd} with the same w and the same group $n=30$ or $n=60$. Comparatively, s_{rd} and n_{rd} perform better than c_{nd} and n_{nd} regarding the correlation coefficients R . Meanwhile, s_{rd} overtakes n_{rd} notably for both $n=30$ and $n=60$, and s_{rd} shows the most prominent correlation with $R_{max} \approx 0.60$ when $w=3\text{km}$ (Figure 8c, Figure 8d). Two phenomena can be observed from the figure. On the one hand, s_{rd} obtains the strongest impact on Δd , which is convincing since s_{rd} incorporates the NO₂ source from roads and NO₂ dispersion following the Gaussian distribution into the correlation. For instance, a long road is likely to produce more NO₂ while a short distance to the station is related to a greater amount of NO₂. On the other hand, $w = 2.25\text{km}$ is an empirical distance that road networks start to have a rather weak impact on Δd .

1
2
3
4
5 354 *3.4. Impacts of regional climates on NO₂ concentration*

6
7 The present study considers that regional climates can also affect the dispersion of NO₂.
8 It is based on the evidence that air temperatures were used to describe urban heat islands
9 and climate largely determines the magnitude of urban heat islands (Manoli *et al.*, 2019;
10 Zhao *et al.*, 2014). As both air temperatures and NO₂ are air properties essentially, NO₂
11 concentrations may also be influenced by climate. To explore the combined impacts of
12 urban mobility and road networks in partition of different climates, the correlation
13 analysis is performed in different climates, namely, *arid* and *humid* climates, *hot* and
14 *cold* climates, and *coastal* and *inland* climates (Figure 9a). The correlation analysis is
15 performed between Δd and $\Delta m_{rd} = s_{rd} \cdot \Delta m_w$, where s_{rd} follows the Gaussian function
16 with $w=3\text{km}$ that obtains the largest R and Δm_w is the change of *workplace* mobility
17 as discussed in Figure 6. Generally, results obtained from $n=30$ (Figures 9b, 9c, 9d) and
18 $n=60$ (Figures 9e, 9f, 9g) are almost the same that $(\Delta d, \Delta m_{rd})$ are strongly correlated.
19 Particularly, the correlations are more prominent in the *arid*, *hot*, and *coastal* climates
20 with $R=\{-0.84, -0.65, -0.77\}$ than in the *humid*, *cold*, and *inland* climates, namely
21 $R=\{-0.60, -0.64, -0.64\}$ (Figure 9b, 9c, 9d). In contrast, correlations based on $n=60$
22 are slightly weaker than $n=30$. That is to say, the *arid*, *hot*, and *coastal* climates tend
23 to facilitate the dispersion of NO₂ based on a given urban mobility and road networks.
24 It is also found that Δm_{rd} shows the most prominent correlation with Δd , and the
25 significance of the correlations decreases from Δm_{rd} with the Gaussian distribution, s_{rd}
26 with the Gaussian distribution (Figure 8d), s_{rd} (Figure 7c), to Δm_w (Figure 6) when
27 they are in the same condition. It suggests that the dynamic mobility constraint by
28 static road networks significantly affects the changes of NO₂ in a large geographical
29 space.
30
31

32
33
34
35
36
37
38 378 **4. Discussion and conclusion**

39
40 An accurate estimation of the time series of NO₂ is essential to predict and investigate
41 the impact of the community mobility on the urban micro-environment. The study
42 refines an established NO₂ prediction model and estimates the NO₂ concentrations
43 without the disruption of COVID-19, which is achieved by incorporating the seasonal
44 and cyclic variations based on years of historical data before 2020. Correlation analysis
45 in this study is performed based on the hypothesis that the predicted level of NO₂
46 after lockdown is larger than the observed level because the lockdown policy leads
47 to less frequent use of vehicles and thus less NO₂ emission while the prediction still
48 follows historical patterns that have not incorporated the dramatic decrease of NO₂
49 after lockdown. Therefore, the changes of urban mobility have shown a causal relation
50 with the difference of NO₂ concentrations between the prediction and observation. The
51 study also suggests that the proposed prediction and analysis method can be used to
52 evaluate the environmental impacts when confronting the COVID-19 pandemic and
53 other public health events.
54
55
56
57
58
59
60

The results suggest that part of the difference between predicted and observed values is the result of the disruptive lockdown measures. During the lockdown period, there are strong and negative correlations between Δd and Δm_{rd} in group of different climates because Δm_{rd} considers the changes of urban mobility, the total length of the roads, and the dispersion following a Gaussian distribution. Two major findings have been generalized as follows. Firstly, a great reduction of urban mobility associated with the *recreation*, *transit*, and *workplace* may result in a considerable decrease in NO₂ in a large geographical area. Secondly, the local climate is also one of the vital factors that have distinct impacts on the dispersion of NO₂. Specifically, the impacts are more prominent for stations in areas where the arid, hot, and coastal climates prevail, since the three climates' correlations are considerably stronger. It is probably because the arid and hot climates would cause uneven air temperatures, which promotes wind ventilation and reduces the NO₂ density, and it is also the case with coastal cities where there are wind cycles between the land and sea. Some features of local weather in terms of daily wind directions and strengths can also mitigate NO₂ concentrations.

The SARIMAX model considers meteorological conditions by establishing exogenous weather variables, such as wind speed and air pressure, optimized by minimizing the AIC value to achieve accurate prediction. Since this study aims to investigate the impacts of mobility on NO₂ concentration, we do not analyze the meteorological influence in detail. Alternatively, we have categorized the analysis into six climate types, which is used as background climate associating with meteorological conditions, to obtain generic phenomenon at a large geographical extent. The prediction with 30 and 60 days before lockdown suggests that instantly seasonal variation influences prediction accuracy, while their effect is insignificant when associating with mobility indicators to explain NO₂ concentration.

In conclusion, the proposed NO₂ difference between prediction and observation is an effective indicator to explain the improvement of the air quality after lockdown. The proposed Δm_{rd} can explain the NO₂ concentration comprehensively by considering the source of dynamic urban mobility, the spatial constraints of road networks, and physical dispersion process. The proposed analysis method can be used to investigate other air quality indicators and other disruptive infectious diseases.

Acknowledgment

Man Sing Wong thanks the funding support from a grant by the General Research Fund (Grant No. 15602619), and the Research Institute for Sustainable Urban Development (Grant No. 1-BBWD), the Hong Kong Polytechnic University. Mei-Po Kwan was supported by a grant from the Research Committee on Research Sustainability of Major RGC Funding Scheme of the Chinese University of Hong Kong. This research is supported by the National Research Foundation, Prime Minister's Office, Singapore under its Campus for Research Excellence and Technological Enterprise (CREATE) programme.

433 References

- 434 Air Quality Open Data Platform, 2020. Air Pollution in World: Real-time Air Quality Index Visual
435 Map. <https://aqicn.org/map/world/>.
- 436 Brauer, M., 2010. How much, how long, what, and where: air pollution exposure assessment for
437 epidemiologic studies of respiratory disease. *Proceedings of the American Thoracic Society* **7** 111–
438 115
- 439 Carslaw, D.C., 2005. Evidence of an increasing NO₂/NO_x emissions ratio from road traffic emissions.
440 *Atmospheric Environment* **39** 4793–4802
- 441 Chan, T.L., Ning, Z., Leung, C.W., Cheung, C.S., et al., 2004. On-road remote sensing of petrol vehicle
442 emissions measurement and emission factors estimation in Hong Kong. *Atmospheric Environment*
443 **38** 2055–2066
- 444 Cohen, A.J., Brauer, M., Burnett, R., Anderson, H.R., et al., 2017. Estimates and 25-year trends of
445 the global burden of disease attributable to ambient air pollution: an analysis of data from the
446 Global Burden of Diseases Study 2015. *The Lancet* **389** 1907–1918
- 447 Congressional Research Service, 2020. Global Economic Effects of COVID-19. <https://fas.org/sgp/crs/row/R46270.pdf>.
- 448 Earth Observatory, 2020. Airborne Nitrogen Dioxide Plummets. <https://earthobservatory.nasa.gov/images/146362/airborne-nitrogen-dioxide-plummets-over-china>.
- 449 Faranda, D., Pons, F.M.E., Giachino, E., Vaienti, S., et al., 2015. Early warnings indicators of
450 financial crises via auto regressive moving average models. *Communications in Nonlinear Science
and Numerical Simulation* **29** 233–239
- 451 Fan, J.L., Da, Y., Zeng, B., Zhang, H., Liu, Z., et al., 2020. *Environmental Research Letters* In Press
452 <https://doi.org/10.1088/1748-9326/abcf76>
- 453 Guan, D., Wang, D., Hallegatte, S., Davis, S.J., Huo, J., et al., 2020. Global supply-chain effects of
454 COVID-19 control measures. *Nature Human Mobility* **4** 557–587
- 455 Greenberg, N., Carel, R.S., Derazne, E., Bibi, H., et al., 2016. Different effects of long-term exposures
456 to SO₂ and NO₂ air pollutants on asthma severity in young adults. *Journal of Toxicology and
Environmental Health A* **79** 342–351
- 457 Google, 2020. COVID-19 Community Mobility Reports. <https://www.google.com/covid19/mobility/>.
- 458 Haiges, R., Wang, Y.D., Ghoshray, A., Roskilly, A.P., 2017. Forecasting electricity generation capacity
459 in Malaysia: an auto regressive integrated moving average approach. *Energy Procedia* **105** 3471–
460 3478
- 461 Heeb, N.V., Saxon, C.J., Forss, A. M. Brühlmann, S., 2008. Trends of NO-, NO₂- , and NH₃-emissions
462 from gasoline-fueled Euro-3-to Euro-4-passenger cars. *Atmospheric Environment* **42** 2543–2554
- 463 He, Q., Qin, K., Cohen, J.B., Loyola, D., Li, D., et al., 2020. Spatially and Temporally Coherent
464 Reconstruction of Tropospheric NO₂ over China combining OMI and GOME-2B measurements.
465 *Environmental Research Letters* In Press <https://doi.org/10.1088/1748-9326/abc7df>
- 466 Hueglin, C., Buchmann, B., Weber, R.O., 2006. Long-term observation of real-world road traffic emission
467 factors on a motorway in Switzerland. *Atmospheric Environment* **40** 3696–3709
- 468 Hyndman, R.J., Khandakar, Y., 2008. Automatic Time Series Forecasting: The forecast Package for
469 R. *Journal of Statistical Software* **27** 107590
- 470 Kucharski, A.J., Russell, T.W., Diamond, C., Liu, Y., Edmunds, J., 2020. Early dynamics of
471 transmission and control of COVID-19: a mathematical modelling study. *The Lancet Infectious
Diseases* **20** 553–558
- 472 Kendrick, C.M., Koonce, P., George, L.A., 2015. Diurnal and seasonal variations of NO, NO₂ and
473 PM_{2.5} mass as a function of traffic volumes alongside an urban arterial. *Atmospheric Environment*
474 **122** 133–141
- 475 Keuken, M., Roemer, M., van den Elshout, S., 2009. Trend analysis of urban NO₂ concentrations and
476 the importance of direct NO₂ emissions versus ozone/NO_x equilibrium. *Atmospheric Environment*
477 **43** 133–141

- 1
2
3
4
5 483 **43** 4780–4783
6 Khaniabadi, Y.O., Goudarzi, G., Daryanoosh, S.M., Borgini, A., et al., 2017. Exposure to PM₁₀, NO₂,
7 and O₃ and impacts on human health. *Environmental Science and Pollution Research* **24** 2781–2789
8 Kurtenbach, R., Kleffmann, J., Niedojadlo, A., Wiesen, P., 2012. Primary NO₂ emissions and their
9 impact on air quality in traffic environments in Germany. *Environmental Sciences Europe* **24** 21
10 Lakhani, A., 2020. Which Melbourne metropolitan areas are vulnerable to COVID-19 based on age,
11 disability and access to health services? Using spatial analysis to identify service gaps and inform
12 delivery. *Journal of Pain and Symptom Management* **60** 41–44
13 Lee, C., 2019. Impacts of urban form on air quality in metropolitan areas in the United States.
14 *Computers, Environment and Urban Systems* **77** 101362
15 Liu, L.J.S., Tsai, M.Y., Keidel, D., Gemperli, A., et al., 2012. Long-term exposure models for traffic
16 related NO₂ across geographically diverse areas over separate years. *Atmospheric environment* **46**
17 460–471
18 Mahato, S., Pal, S., Ghosh, K.G., 2020. Effect of lockdown amid COVID-19 pandemic on air quality
19 of the megacity Delhi, India. *Science of The Total Environment* **730** 139086
20 Manoli, G., Fatichi, S., Schläpfer, M., Yu, K., et al., 2019. Magnitude of urban heat islands largely
21 explained by climate and population. *Nature* **573** 55–60
22 Meng, X., Chen, L., Cai, J., Zou, B., et al., 2015. A land use regression model for estimating the NO₂
23 concentration in Shanghai, China. *Environmental Research* **137** 308–315
24 Minoura, H., Ito, A., 2010. Observation of the primary NO₂ and NO oxidation near the trunk road in
25 Tokyo. *Atmospheric Environment* **44** 23–29
26 Mohegh, A., Goldberg, D., Achakulwisut, P., Anenberg, S.C., 2020. Sensitivity of estimated NO₂-
27 attributable pediatric asthma incidence to grid resolution and urbanicity. *Environmental Research
Letters* In Press <https://doi.org/10.1088/1748-9326/abce25>
28 National Weather Service, 2020. Addition Köppen-Geiger Climate Subdivisions. https://www.weather.gov/jetstream/climate_max.
29 Open Weather, 2020. We Deliver 2 Billion Forecasts Per Day. <https://openweathermap.org/>.
30 OpenStreetMap, 2020. A map of the world under an open license. <https://www.openstreetmap.org>.
31 Palmgren, F., Berkowicz, R., Ketzel, M. Winther, M., 2007. Elevated NO₂ pollution in Copenhagen
32 due to direct emission of NO₂ from road traffic. In 2nd ACCENT Symposium, Urbino, Italy, July
33 23–27.
34 Shon, Z.H., Kim, K.H., Song, S.K., 2011. Long-term trend in NO₂ and NO_x levels and their emission
35 ratio in relation to road traffic activities in East Asia. *Atmospheric Environment* **45** 3120–3131
36 Shrestha, A. M., Shrestha, U.B., Sharma, R., Bhattachari, S. et al., 2020. Lockdown
37 caused by COVID-19 pandemic reduces air pollution in cities worldwide. *EarthArXiv*.
38 <https://doi.org/10.31223/osf.io/edt4j>
39 Singh, S.N., Mohapatra, A., 2019. Repeated wavelet transform based ARIMA model for very short-term
40 wind speed forecasting. *Renewable Energy* **136** 758–768
41 Singer, G., Zivin, J.G., Neidell, M., Sanders, N., 2020. Air Pollution Increases Influenza
42 Hospitalizations. *medRxiv*. <https://doi.org/10.1101/2020.04.07.20057216>
43 State Space Methods, 2020. Seasonal AutoRegressive Integrated Moving Average with eX-
44ogenous regressors model. <https://www.statsmodels.org/dev/generated/statsmodels.tsa.statespace.sarimax.SARIMAX.html>.
45 Tang, J., McNabola, A., Missellar, B., Pilla, F., et al., 2019. Assessing the impact of vehicle speed
46 limits and fleet composition on air quality near a school. *International Journal of Environmental
Research and Public Health* **16** 149
47 UN News, 2020. UN launches COVID-19 plan that could ‘defeat the virus and build a better world’.
48 <https://news.un.org/en/story/2020/03/1060702>.
49 Valipour, M., 2015. Long-term runoff study using SARIMA and ARIMA models in the United States.
50 *Meteorological Applications* **22** 592–598
51 Venter, Z.S., Aunan, K., Chowdhury, S. Lelieveld, J., 2020. COVID-19 lockdowns cause global air
52
53
54
55
56
57
58
59
60

- 1
2
3
4
5 pollution declines. *PNAS* **117** 18984–18990
6 Velders, G.J., Diederens, H.S., 2009. Likelihood of meeting the EU limit values for NO₂ and PM₁₀
7 concentrations in the Netherlands. *Atmospheric Environment* **43** 3060–3069
8 Wang, Y., Bechle, M.J., Kim, S.M., Adams, P.J., et al., 2020. Spatial decomposition analysis of NO₂
9 and PM_{2.5} air pollution in the United States. *Atmospheric Environment* **241** 117470
10 Zhu, Y., Jinggu, X., Fengming, H., Liqing, C., 2020. Association between short-term exposure to air
11 pollution and COVID-19 infection: Evidence from China. *Science of The Total Environment* **727**
12 138704
13 Zhao, L., Lee, X., Smith, R.B., Oleson, K., 2014. Strong contributions of local background climate to
14 urban heat islands. *Nature* **511** 216–219
15
16
17
18
19
20
21
22
23
24
25
26
27
28
29
30
31
32
33
34
35
36
37
38
39
40
41
42
43
44
45
46
47
48
49
50
51
52
53
54
55
56
57
58
59
60